Salt Diapirism in Europa's Periodically Thickening Icy Shell

Mariam Helal[1], Elvira Mulyukova[2]
[1]University of California, Berkeley, Department of Astronomy and Department of Earth & Planetary Science
[2]Northwestern University, Department of Earth , Environmental, and Planetary Sciences

What we know and don't know about Europa

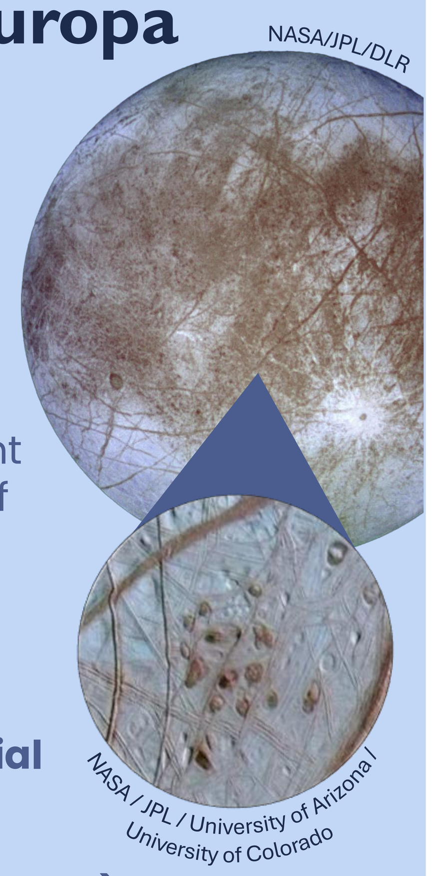

Knowns:

- Europa is one of Jupiter's large icy moons
- Salty, potentially habitable, subsurface ocean
- Sources of internal heat: tidal flexing and radioactive decay
- **Varying ice shell thickness due to orbital cycles**

Unknowns:

- Observed dome and spot-like surface features, called lenticulae, suggest some degree of element cycling between surface and interior, the extent of which is uncertain [1]
- Large source of uncertainty is behavior of the ice shell, which is the primary barrier in transporting heat, chemical species, and material as a whole

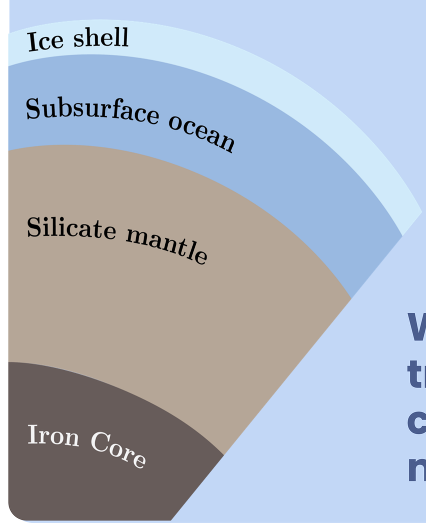

We estimate the contribution of salt diapirism to material transfer in Europa's ice shell. To do this, we couple the continuum scale model of density-driven flow and microphysical creep models of crystalline materials (i.e., ice).

Hypothesis: Different ice growth rates manifest in different diapir shapes and ascent rates

A basal ice layer freezes out of ocean during periods of ice shell growth. Our key assumption is that differences in ice growth rates have cascading effects on the physical properties of the basal ice layer, therefore producing different types of diapirs. For example, faster ice growth rates lead to:

- Thicker basal layer (h)
- Smaller crystalline grain sizes (R_L)
- Smaller viscosity (μ_L)
- More salt entrained (C_L)
- Smaller density contrast $(\Delta\rho)$

$$h = \frac{\Delta h}{\Delta t} P_{growth} \quad \textbf{Eq. 1}$$

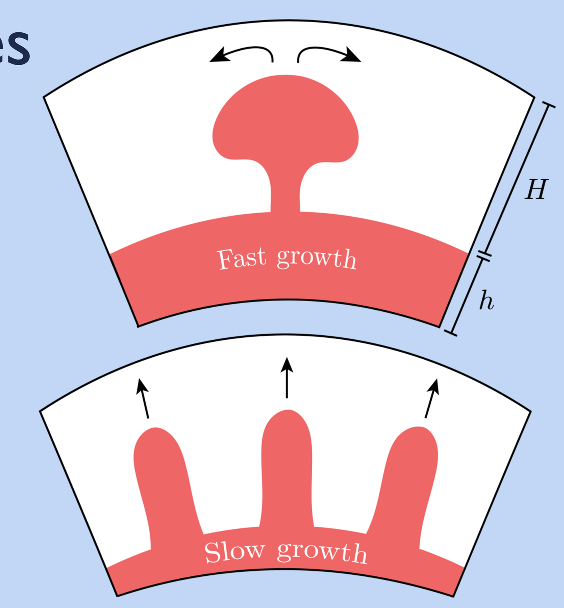

Methods: Physical inputs and workflow

Parameter	Value	Units	Definition
L	100	km	Horizontal length scale of the modeled region.
H	40	km	Ice shell thickness.
$\Delta h/\Delta t$	2.5×10^{-11} or varied	m s^{-1}	Ice shell growth rate.
$P_{\rm growth}$	75	Ma	Timescale over which the ice shell grows.
$C_{\rm ice}$	14.72	ppt	Salt concentration in the overlying ice shell.
C_L	1.053	ppt	Salt concentration in basal ice layer.
$R_{\rm ice}$	1	mm	Grain size of the overlying ice shell.
R_L	1 or varied	mm	Grain size of the basal ice layer.
σ	10^3	Pa	Applied shear stress.
$\rho_{\rm pure}$	917	kg m^{-3}	Density of pure ice.
$\rho_{\rm salt}$	1300	kg m^{-3}	Density assigned to the salt component in the linear mixing model.
h	Eq. 1	m	Thickness of the basal ice layer.
ρ_L	Eq. 5 or varied	kg m^{-3}	Density of the basal ice layer
$\rho_{\rm ice}$	Eq. 5	kg m^{-3}	Density of the overlying ice shell.
$\mu_{\rm ice}$	Eqs. 2–4 or varied	Pa s	Effective viscosity of the overlying ice shell.
μ_L	Eqs. 2–4	Pa s	Effective viscosity of the basal ice layer.

Table 1: A table of the default model parameters and their definitions. Parameters with given values are prescribed, while others are calculated through the listed equations. Parameters that are varied in certain runs of the model are stated to be so.

Model Part 1: Use $\Delta h/\Delta t$ and ice physics to determine physical properties of the ice.
Model Part 2: Use Rayleigh-Taylor framework to find diapir spacing and size.
Model Part 3: Determine the diapir ascent time, assuming they rise at Stokes velocity.

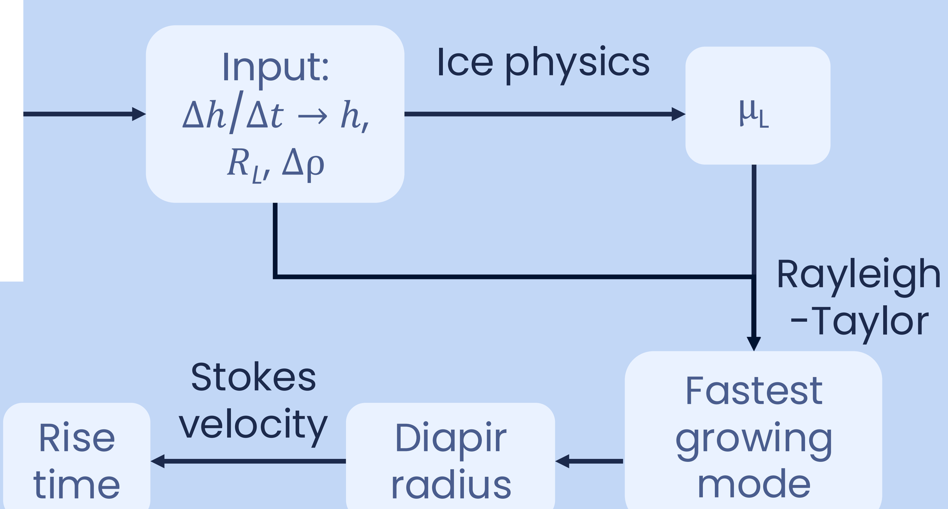

Model Part 1: Ice physics and deformation

The ice shell deforms by solid-state creep, which can be accommodated by different micro-mechanisms. Diffusion creep (Eq. 3) and grain boundary sliding are sensitive to grain size, whereas dislocation creep and basal slip are not. These deformation mechanisms all contribute to the effective viscosity of the ice (see Eq. 2-4). Salt impurities influence viscosity through pinning grain boundaries, capping grain size [3]. Additionally, they determine the density of the basal ice layer through Eq. 5 in model runs when ρ_L is not treated as a coupled.

$$\mu_i = \frac{R^{m_i}}{2A_i}\sigma^{1-n_i}\exp\left(\frac{E_i}{R_G T}\right) \quad \textbf{Eq. 2}$$

$$\mu_{\rm diff} = \frac{1}{2}\left(\frac{3R_G T_b R^2}{42 V_m D_{\rm diff}}\right)\exp\left(\frac{E_{\rm diff}}{R_G T}\right) \quad \textbf{Eq. 3}$$

$$\mu_{tot} = \left(\frac{1}{\mu_{\rm diff}} + \frac{1}{\mu_{\rm disl}} + \frac{1}{\mu_{\rm gb}+\mu_{\rm bs}}\right)^{-1} \quad \textbf{Eq. 4}$$

$$\rho = \left(1 - \frac{C}{1000}\right)\rho_{\rm pure} + \frac{C}{1000}\rho_{\rm salt} \quad \textbf{Eq. 5}$$

Model Part 2: Rayleigh-Taylor instability

We use the Rayleigh-Taylor instability framework to describe the initial geometry development of the buoyant basal layer, which eventually forms diapirs [2]. Some perturbation described by a waveform exists in the interface between the basal layer and older ice shell. The fastest growing mode informs the spacing between diapirs, and thus their size.

$$\tau = \frac{K\mu_1}{g\Delta\rho h}\left[\frac{\sinh K + K + \left(\frac{\mu_{\rm ice}}{\mu_L}\right)(2\cosh K) + \left(\frac{\mu_{\rm ice}}{\mu_L}\right)^2(\sinh K - K)}{\cosh K - 1 + \left(\frac{\mu_{\rm ice}}{\mu_L}\right)(\sinh K - K)}\right] \quad \textbf{Eq. 6}$$

$K = 2kh$ **Eq. 7** $\qquad k = \pi/\lambda$ **Eq. 8**

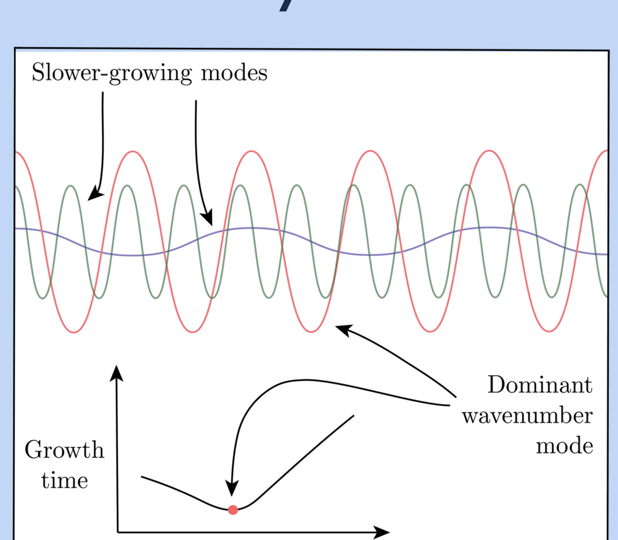

Model Part 3: Diapir rise at Stokes velocity

The Hadamard–Rybczynski Stokes velocity (Eq. 10) is calculated based on radius of the diapirs. Eq. 9 is then used to determine the time it takes the diapir to cross H.

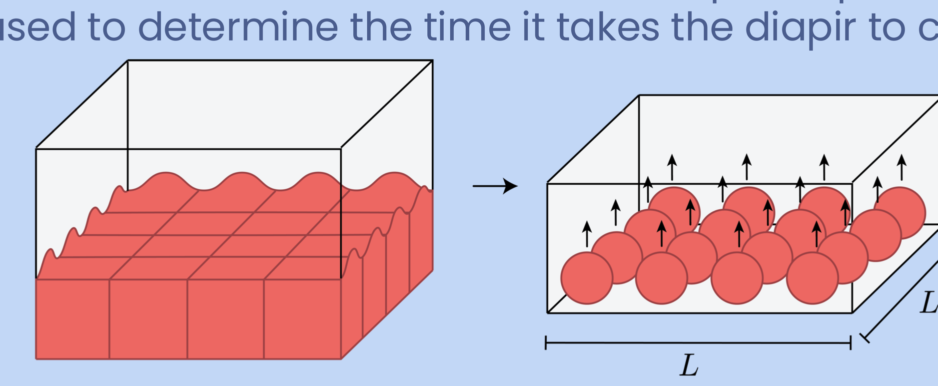

$$t_{\rm rise} = \frac{H}{v} \quad \textbf{Eq. 9}$$

$$v = \frac{2\Delta\rho g R_D^2}{3\mu_{\rm ice}}\left(\frac{\mu_{\rm ice}+\mu_L}{2\mu_{\rm ice}+3\mu_L}\right) \quad \textbf{Eq. 10}$$

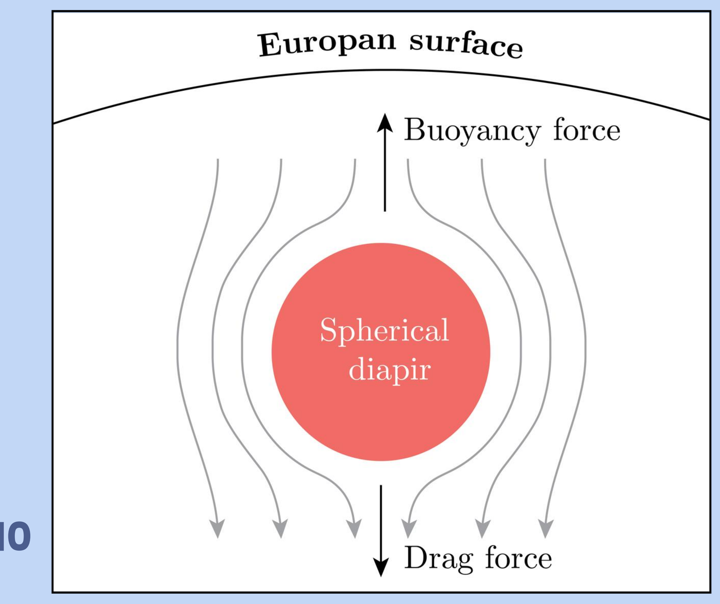

Results: Parameter coupling impacts rise time

Reference:

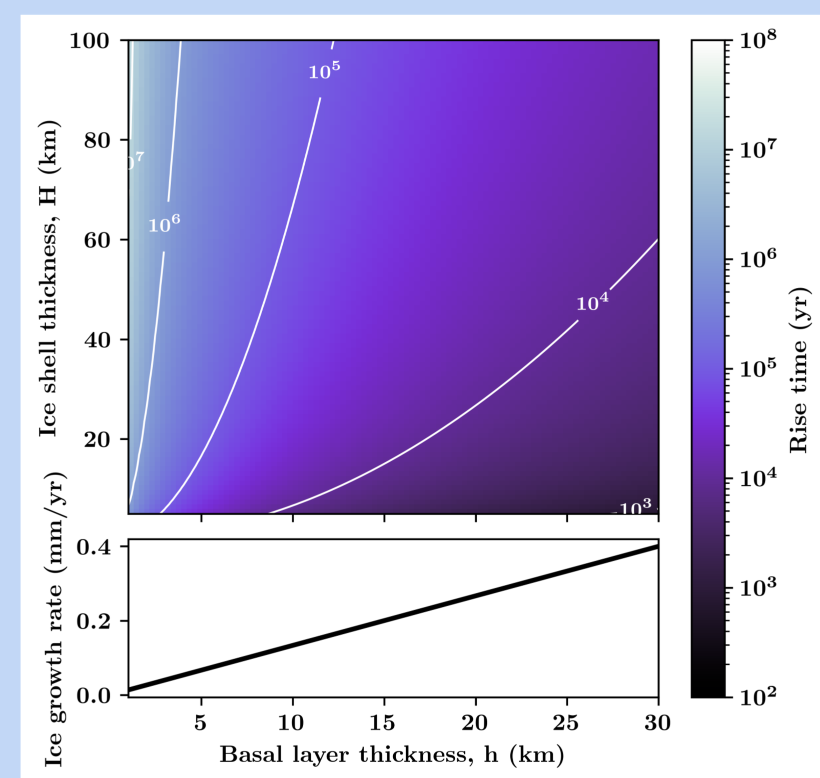

Figure 1: A reference heatmap illustrating how h and H impact t_{rise}, with all other parameters kept constant. As expected, a larger H means it takes longer for the diapir to traverse the shell, according to Eq. 9. A larger h produces a larger diapir, which increases the Stokes velocity according to Eq. 10, therefore decreasing t_{rise}. The bottom plot shows how ice growth rate varies with h for a fixed P_{growth}.

The results show that coupling ρ_L and h introduces a maximum diapir size, the exact value for which changes when introducing coupling between R_L and h.

Coupling between ρ_L and h:

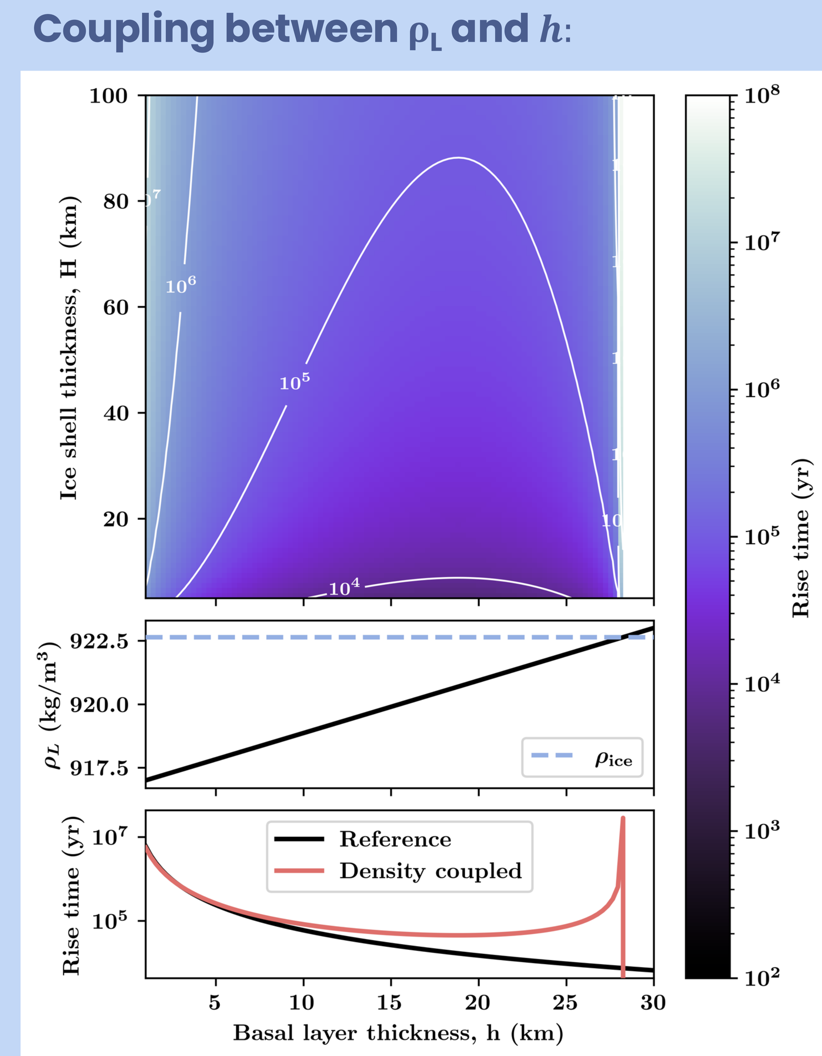

Figure 2: We introduce a coupling between ρ_L and h, where ρ_L increases with h. Because $\Delta\rho$ does not impact the dominant wavelength, the observed deviation from the reference is due to the dependance of v on $\Delta\rho$ (Eq. 10). This coupling works to dampen the effect of h alone on the t_{rise}. A discontinuity is seen when $\rho_L \geq \rho_{ice}$ due to $\Delta\rho$ no longer being positive, stopping diapirism.

Additional coupling between R_L and h:

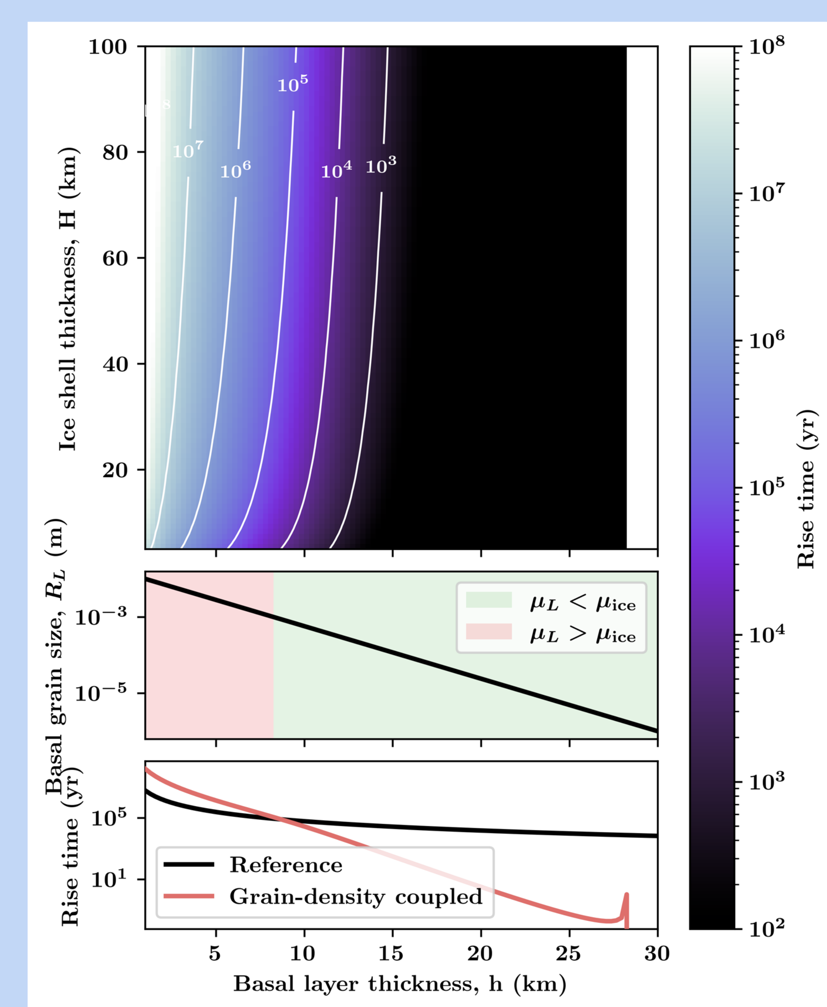

Figure 3: We introduce an additional coupling between R_L and h, where R_L decreases with h. The variation in R_L influences μ_L (Eq. 2-4), an input in both the dominant wavelength used to determine diapir radius as well as v (Eq. 10). The regime in which t_{rise} is larger or smaller than the reference depends on whether $\mu_L > \mu_{ice}$. σ is kept constant for the sake of simplicity.

Conclusions & future work

Figures 1 , 2, and 3 show that across a range of parameters, **diapir rise occurs on geologically relevant timescales**. This supports previous studies that claim salt diapirism as a potential driver of the production of lenticulae. Figures 2 and 3 shows that the **coupling of ρ_L and h works to place an upper limit on the size of diapirs, a conclusion that can be directly tied to observations of lenticulae size.** Figure 3 shows that coupling R_L and h makes t_{rise} more sensitive to h, with low viscosity diapirs forming from a thicker layer and rising faster. Eventually, the ρ_L coupling reverses the trend again, but now at a different maximum diapir size compared to the scenario where R_L and h are not coupled (Figure 2).

Future work will introduce further complexity to the model, particularly by replacing the linear coupling model with more physically accurate coupling mechanisms.

References

[1] Pappalardo, R. T., & Barr, A. C. 2004, Geophysical Research Letters, 31, doi: 10.1029/2003GL019202
[2] Whitehead Jr., J. A., & Luther, D. S. 1975, Journal of Geophysical Research (1896-1977), 80, 705, doi: 10.1029/JB080i005p00705
[3] Durham, W. B., Prieto-Ballesteros, O., Goldsby, D. L., & Kargel, J. S. 2010, Space Science Reviews, 153, 273, doi: 10.1007/s11214-009-9619-1

Acknowledgments

Thank you to the CIERA REU program for providing the space and support for this project. This material is based upon work supported by the U.S. National Science Foundation (NSF) under Award Number AST-2446392. Any opinions, findings, and conclusions or recommendations expressed in this material are those of the author(s) and do not necessarily reflect the views of the NSF.